

Quantum Virtual Cooling

Jordan Cotler,^{1,*} Soonwon Choi,² Alexander Lukin,³ Hrant Gharibyan,¹ Tarun Grover,⁴ M. Eric Tai,³ Matthew Rispoli,³ Robert Schittko,³ Philipp M. Preiss,^{3,5} Adam M. Kaufman,^{3,6} Markus Greiner,³ Hannes Pichler,^{7,3} and Patrick Hayden¹

¹*Stanford Institute for Theoretical Physics, Stanford University, Stanford, CA 94305, US*

²*Department of Physics, University of California, Berkeley, CA 94720, USA*

³*Department of Physics, Harvard University, Cambridge, MA 02138, USA*

⁴*Department of Physics, University of California at San Diego, La Jolla, CA 92093, USA*

⁵*Physics Institute, Heidelberg University, 69120 Heidelberg, Germany*

⁶*JILA, National Institute of Standards and Technology and University of Colorado, and Department of Physics, University of Colorado, Boulder, Colorado 80309, USA*

⁷*ITAMP, Harvard-Smithsonian Center for Astrophysics, Cambridge, MA 02138, USA*

(Dated: June 16, 2022)

We propose a quantum information based scheme to reduce the temperature of quantum many-body systems, and access regimes beyond the current capability of conventional cooling techniques. We show that collective measurements on multiple copies of a system at finite temperature can simulate measurements of the same system at a lower temperature. This idea is illustrated for the example of ultracold atoms in optical lattices, where controlled tunnel coupling and quantum gas microscopy can be naturally combined to realize the required collective measurements to access a lower, virtual temperature. Our protocol is experimentally implemented for a Bose-Hubbard model on up to 12 sites, and we successfully extract expectation values of observables at half the temperature of the physical system. Additionally, we present related techniques that enable the extraction of zero-temperature states directly.

PACS numbers: 03.67.a, 03.65.Ud, 03.67.Bg, 03.75.Dg, 05.30.Jp, 05.30.Fk

INTRODUCTION

Quantum simulators have been proposed to understand the complex properties of strongly correlated quantum many-body systems [1–3]. Significant progress has been made in building both analog and digital quantum simulators with a variety of quantum optical systems [4–11]. A particularly successful approach is to use cold neutral atoms in optical lattices to emulate the physics of interacting electrons in solid state systems [2, 12–19]. This is exemplified by recent experimental advances that enable the exploration of quantum magnetism [20–26], measurement of many-body entanglement [27–29], and study of quantum dynamics out of equilibrium with bosonic and fermionic atoms [28, 30–32, 34]. One of the central, outstanding challenges in these experiments is to reach temperatures that are low enough to observe many stipulated quantum phases [2]. Even though there has been much recent progress, e.g., via entropy redistribution techniques [26, 35–37], the observation of extremely low temperature phenomena such as d-wave superconductivity or fractional quantum Hall physics remains elusive.

In this work, we develop a novel approach to address this issue by introducing a measurement scheme that enables to access system properties at fractions of its temperature T . This “virtual” cooling to a temperature $T_{\text{virtual}} = T/n$ ($n = 2, 3, \dots$) is facilitated by joint measurements on n copies of the system. A schematic is given in Fig. 1(a). Further, we detail implementations tailored

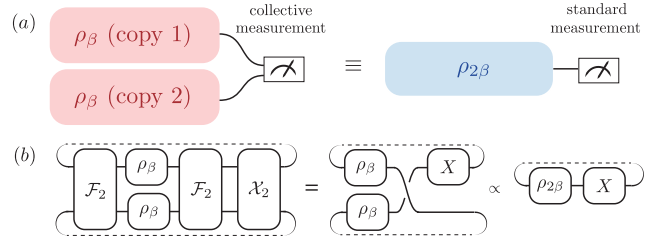


FIG. 1: (a) Schematic representation of the virtual cooling protocol. Collective measurements on two copies of a thermal state ρ_β at temperature $T = 1/(k_B\beta)$ correspond to standard measurements at half the temperature, $T/2$. (b) Diagrammatic representation. Two copies are evolved with the unitary \mathcal{F}_2 , and a subsequent measurement of \mathcal{X}_2 is performed. In combination this gives the expectation value $\text{tr}\{\rho_{2\beta} X\}$ corresponding to half the original temperature.

to cold-atom systems in optical lattices, and illustrate our protocol in an experimental quantum simulation of the Bose-Hubbard model. Finally, we show how these ideas can be generalized and discuss protocols to distill the many-body ground state from multiple copies of thermal many-body states.

We are interested in quantum many-body systems described by a thermal state $\rho(T) = e^{-\beta H}/Z$, where H is the Hamiltonian of the system and $Z(T) = \text{tr}\{e^{-\beta H}\}$ is the partition function at inverse temperature $\beta = 1/(k_B T)$. The measurement of an observable X in the state ρ gives the expectation value $\langle X \rangle_T = \text{tr}\{X\rho\}$. Be-

low we will discuss a protocol that allows us to effectively measure $\langle X \rangle_{T/n}$. The central idea is based on the ability to express the thermal density operator at T/n by the n -th power of $\rho(T)$

$$\rho(T/n) = \rho(T)^n / \text{tr}\{\rho(T)^n\}. \quad (1)$$

In order to access the higher powers of the thermal state, we require n copies of the state $\rho(T)$ prepared in parallel as well as the capability to implement operations that exchange the n copies. More specifically, we have $\text{tr}\{X\rho^n\} = \text{tr}\{X_s S_n \rho^{\otimes n}\}$, where S_n cyclically permutes quantum states in the n copies, i.e. $S_n|\psi_1\rangle \otimes |\psi_2\rangle \otimes \cdots \otimes |\psi_n\rangle = |\psi_2\rangle \otimes |\psi_3\rangle \otimes \cdots \otimes |\psi_1\rangle$, and X_s is the symmetrized embedding of X on the n -fold replicated Hilbert space $X_s = \frac{1}{n} \sum_{m=1}^n S_n^m (X \otimes \mathbf{1}^{\otimes(n-1)}) S_n^{m\dagger}$. Therefore, the virtual measurement of $\langle X \rangle_{T/n}$ at temperature T/n via Eqn. (1) can be reduced to determining the expectation values $\langle X_s S_n \rangle$ and $\langle S_n \rangle$ on the n copies of the state at temperature T . This is illustrated in Fig. 1(b). Measurements of expectation values of S_n can be achieved with auxiliary qubits [38, 39], or directly via many-body state interferometry [40–42], as recently demonstrated with cold atoms [27]. We also note that our protocols apply to subsystems which are locally thermal, even if the global system is not thermal. In our experiments below, we leverage ‘eigenstate thermalization’ [43–47] to obtain thermal reduced density matrices from globally pure states of finite energy density in a chaotic system. Earlier theoretical work provided numerical evidence that a chaotic eigenstate or a reduced density matrix of a thermal state encodes correlations at all temperatures [48, 49].

Below, we discuss protocols to measure $\langle X_s S_n \rangle$ for arbitrary n and detail the procedure for the simplest example $n = 2$. We first focus on an interferometric measurement scheme and demonstrate that it can be implemented in current experiments with cold atoms. Alternative virtual cooling schemes using ancillary atoms are discussed in the Supplementary Materials. Finally, we show that schemes with ancillary atoms can be generalized to not only virtually cool a many-body system, but directly distill and prepare the many-body ground state from a thermal state. Importantly, all of the discussed protocols are agnostic to the temperature T of the physical system, and thus can be used to obtain additional, virtual cooling even after all available physical cooling methods have been deployed.

INTERFEROMETRIC MEASUREMENT

To simplify the presentation we first discuss a virtual cooling scheme for bosonic atoms in optical lattices. The key idea is to represent the permutation operator S_n in the bosonic Hilbert space as $S_n = \mathcal{F}_n \mathcal{R}_n \mathcal{F}_n^\dagger$, where the

unitary \mathcal{F}_n denotes the discrete Fourier transformation

$$\mathcal{F}_n a_{p,j} \mathcal{F}_n^\dagger = \frac{1}{\sqrt{n}} \sum_{k=1}^n e^{i \frac{2\pi k p}{n}} a_{k,j} \quad (2)$$

and $\mathcal{R}_n = \prod_j e^{-i 2\pi/n \sum_{p=1}^n p n_{p,j}}$ [56]. Here $a_{p,j}$ denotes the bosonic annihilation operator on site j in copy p , and $n_{p,j} = a_{p,j}^\dagger a_{p,j}$ is the corresponding number operator. Note that \mathcal{F}_n can be realized by simply introducing tunnel coupling between neighboring copies [41], and \mathcal{R}_n can be directly measured with a number-resolving quantum gas microscope. This representation of the permutation operator suggests that we introduce an operator $\mathcal{X}_n = \mathcal{F}_n X_s \mathcal{F}_n^\dagger$, which is the discrete Fourier transform of the observable X that we want to measure. With this definition we can express

$$\langle X \rangle_{T/n} = \text{tr}\{\mathcal{X}_n \mathcal{R}_n (\mathcal{F}_n \rho^{\otimes n} \mathcal{F}_n^\dagger)\} / \text{tr}\{\mathcal{R}_n (\mathcal{F}_n \rho^{\otimes n} \mathcal{F}_n^\dagger)\}. \quad (3)$$

A measurement of X at the virtually reduced temperature T/n thus consists of a measurement of $\mathcal{X}_n \mathcal{R}_n$ and \mathcal{R}_n after application of the discrete Fourier transform across the copies. For many interesting observables one finds $[\mathcal{X}_n, \mathcal{R}_n] = 0$ so that \mathcal{R}_n and \mathcal{X}_n can be measured independently.

As a specific example, we consider the experimentally simplest case $n = 2$ and the measurement of the on-site density by choosing $X \equiv n_j$. The corresponding protocol consists of three steps. (i) We prepare $n = 2$ identical instances of the thermal many-body state $\rho(T)$. This can be achieved, for example, by preparing two identical states in neighboring 1D tubes, or 2D planes. It is essential that the copies are decoupled at this stage, which can be achieved by using a large optical potential between the tubes or planes to suppress any inter-copy tunneling. (ii) We then freeze the dynamics within each copy, and lower the potential between the two copies, e.g. using an optical superlattice. This induces tunneling between the two copies via the Hamiltonian $H_{BS} = -J_{BS} \sum_j (a_{1,j}^\dagger a_{2,j} + \text{h.c.})$, which allows us to realize the so-called beamsplitter operation \mathcal{F}_2 that maps $\rho^{\otimes 2} \rightarrow \mathcal{F}_2 \rho^{\otimes 2} \mathcal{F}_2^\dagger$. Interactions between the atoms need to be turned off (e.g. via a Feshbach resonance) or made negligible as compared to J_{BS} during this step. (iii) Finally, we measure the on-site occupation number on all sites in both copies using a number-resolving quantum gas microscope. This gives direct access to $\mathcal{R}_2 = (-1)^{\sum_j n_{1,j}}$ and $\mathcal{X}_2 = \mathcal{F}_2 \frac{1}{2} (n_{1,j} + n_{2,j}) \mathcal{F}_2^\dagger = \frac{1}{2} (n_{1,j} + n_{2,j})$. Averaging the results over multiple experiments gives the expectation value of the local density at $T/2$ via Eqn. (3) (for a schematic of a single measurement trial, see Fig. 2(a) below). Remarkably, this experimental procedure parallels the one employed to determine the second order Rényi entropy of cold atoms, with atom number-resolved measurements being the only additional requirement. Such measurements were first demonstrated for

one-dimensional systems using full-atom-number-resolved imaging in quantum gas microscope [28].

EXPERIMENTAL DEMONSTRATION

In order to demonstrate our protocol, we experimentally realize it in a one-dimensional Bose-Hubbard model. In the experiment, a Bose-Einstein condensate of ^{87}Rb atoms is loaded into a two-dimensional optical lattice positioned at the focus of a high-resolution imaging system. The dynamics of the atoms is well-described by a Bose-Hubbard Hamiltonian parametrized by tunneling strength J and on-site interaction energy U (see Ref. [28] for details).

The experimental protocol consists of four steps: initialization, quenched thermalization dynamics, beam-splitter operations, and measurements. During initialization, optical potentials are sequentially manipulated in order to isolate an initial product state, $|\psi_0\rangle$, with a single atom on the central 2×6 sites of a $2 \times L$ plaquette in the deep $45E_r$ lattice where the tunneling between the sites is negligible [28]. Each $1 \times L$ tube represents an identical copy of the system. Next, the lattice potential along the chains is suddenly lowered, allowing particles to tunnel and interact within each chain. It has been previously shown [28] that this quenched dynamics drives the thermalization of small subsystems within the chain. Hence, after sufficiently long time evolution, the state of the subsystem can be described by an effective temperature T and chemical potential μ , which are determined by the total energy and particle number density of $|\psi_0\rangle$. (See also [49].) After the desired time evolution the dynamics of the system is frozen by suddenly increasing the lattice depth along the chains, and a beamsplitter operation \mathcal{F}_2 is implemented by lowering the potential barrier between the two chains, such that particles can tunnel (in the transverse direction) for a prescribed time. Finally, the number of particles on each individual lattice site is measured. This procedure is repeated multiple times in order to obtain sufficient statistics.

We apply our virtual cooling protocol in three regimes (A, B, and C), with differing initial states $|\psi_0\rangle$, system size L , and Hamiltonian parameters U/J . For the data sets A and B, each of $L = 6$ sites is initially occupied by one particle, whereas for the data set C, only the middle six out of the total $L = 12$ sites are occupied by one particle per site. The tunneling rates are set such that $U/J \approx 1.56$ (data set A) or 0.33 (data sets B and C). These combinations lead to the effective temperatures and chemical potentials $(T/J, \mu/J) \approx (3.5, -1.0)$, $(11.5, -6.3)$, and $(18.3, -17.7)$ of subsystems for data sets A, B, and C, respectively. Based on our protocol, we extract the average particle number density $\langle n_i \rangle$ for thermal ensembles at reduced temperature.

Fig. 2(b) shows the resulting single-site particle density

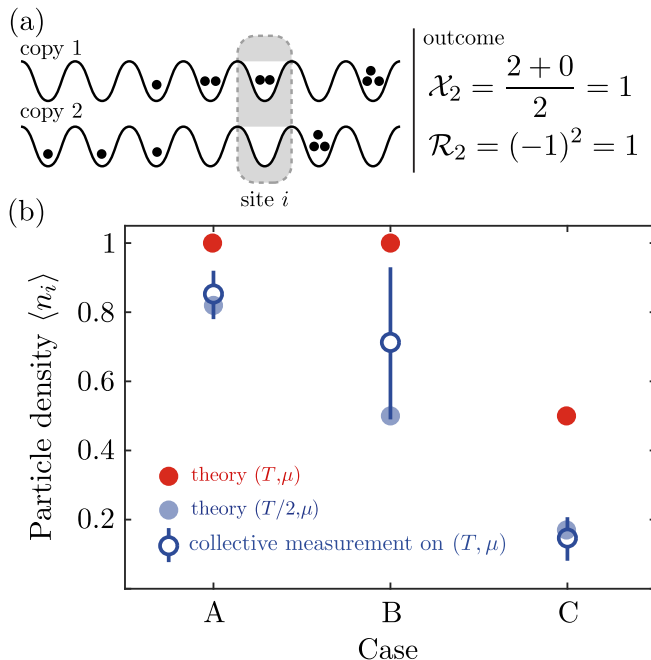


FIG. 2: (a) Schematic for a single measurement trial of $\mathcal{X}_2 = \frac{1}{2}(n_{1,i} + n_{2,i})$ and \mathcal{R}_2 restricted to the i th site, after \mathcal{F}_2 has been applied to the two copies. (b) Measured single-site density, averaged over all but the edge sites of the chain, after virtual cooling has been applied to the system (blue circles with vertical error bars). Red discs show the single-site density of the state before our protocols are utilized (the actual density of particles in each experiment), whereas light blue discs correspond to the prediction of the effective thermal ensemble (see text) at half the temperature. Agreement of the data with the reduced-temperature ensemble validates the applicability of our method in the experimental system. Error bars denote the standard error of the mean.

after virtual cooling for all three cases. We compare these results with the initial single-site density at the original temperatures as well as theoretical predictions from an ideal thermal ensemble $\rho_{2\beta}$ at half of the original temperatures. All data points are in good agreement with the reduced temperature ensemble indicating that our virtual cooling scheme works in the experimental system.

OBSERVABLES

In our experiment, we measured the single-site density of bosons in an optical lattice at half the physical temperature. If we measure the single-site density on the j th site, we have $X \equiv n_j$, $X_s = \frac{1}{2}(n_{1,j} + n_{2,j})$, and $\mathcal{X}_2 = \mathcal{F}_2 \frac{1}{2}(n_{1,j} + n_{2,j}) \mathcal{F}_2^\dagger = \frac{1}{2}(n_{1,j} + n_{2,j})$. Notice that $X_s = \mathcal{X}_2$, since each operator is invariant under the many-body Fourier transform \mathcal{F}_2 between the two system copies. Here, \mathcal{X}_2 is easily measured by averaging the number of atoms on the j th site in the two copies. Furthermore, \mathcal{X}_2 commutes with \mathcal{R}_2 , and so we can measure

the observables in either order. In fact, \mathcal{X}_2 and \mathcal{R}_2 commute with all single-site densities $n_{1,j}$, $n_{2,k}$, and so we can simply measure the individual particle numbers and combine them to compute the expectation values of \mathcal{X}_2 and \mathcal{R}_2 .

For more complicated observables such as density-density correlators $X \equiv n_j n_\ell$, the situation is more subtle. A direct application of the procedure outlined above requires a measurement of

$$\begin{aligned} \mathcal{X}_2 &= \mathcal{F}_2 \frac{1}{2} (n_{1,j} n_{1,\ell} + n_{2,j} n_{2,\ell}) \mathcal{F}_2^\dagger \\ &= \frac{1}{4} (n_{1,j} + n_{2,j}) (n_{1,\ell} + n_{2,\ell}) \\ &\quad + \frac{1}{4} (a_{1,j}^\dagger a_{2,j} + a_{2,j}^\dagger a_{1,j}) (a_{1,\ell}^\dagger a_{2,\ell} + a_{2,\ell}^\dagger a_{1,\ell}). \end{aligned} \quad (4)$$

While the first term in Eqn. (4) (i.e., the final equality) is easily measurable with standard quantum gas microscopy, the second term requires additional interferometric apparatus.

However, the first term of Eqn. (4) by itself contains interesting information about the system at half of its temperature. This first term of Eqn. (4) is easy to measure, since it commutes with \mathcal{R}_2 and all of the number operators. Doing so would output the unconventional correlator

$$\frac{1}{2} \text{tr}\{n_j n_\ell \rho(T/2)\} + \frac{1}{2} \frac{\text{tr}\{n_j \rho(T) n_\ell \rho(T)\}}{\text{tr}\{\rho(T)^2\}}. \quad (5)$$

The term on the left here is the desired equal-time density-density correlator at half the system temperature, whereas the term on the right is peculiar. In fact, this peculiar term is equal to the *unequal imaginary-time* correlator $\frac{1}{2} \text{tr}\{n_j(1/T) n_\ell \rho(T/2)\}$ where $n_j(\tau) = e^{H\tau} n_j e^{-H\tau}$ is the number density evolved in imaginary time. If our system is translation invariant and at sufficiently low temperature, we expect $\text{tr}\{n_j n_\ell \rho(T/2)\}$ to depend on $|j - \ell|$, whereas the peculiar term should not strongly depend on $|j - \ell|$. This is because at low temperatures, the large imaginary time evolution of the operator n_j scrambles it strongly, destroying the memory of its initial position j . Indeed, in the limit of $T \rightarrow 0$, the peculiar term is just $\langle \psi_0 | n_j | \psi_0 \rangle \langle \psi_0 | n_\ell | \psi_0 \rangle$ which is clearly independent of $|j - \ell|$. At high temperature and small $|j - \ell|$, both terms in Eqn. (5) have a nontrivial dependence on $|j - \ell|$ and so we are unable to extract each term separately. Nevertheless, it is interesting to note that our protocol yields some information about the unequal imaginary-time correlator in this regime. We note also that when $|j - \ell|$ is much larger than the thermal correlation length, both terms in Eqn. (5) approach $\frac{1}{2} \text{tr}\{n_j \rho(T/2)\} \text{tr}\{n_\ell \rho(T/2)\}$. We explore the dependence of $\text{tr}\{n_j \rho(T) n_\ell \rho(T)\}$ on $|j - \ell|$ as a function of T in the Supplementary Materials, and confirm that there is essentially no dependence at sufficiently low temperatures.

Another approach to measuring density-density correlators is to use a different protocol involving an ancillary qubit to implement a controlled swap operation (see Supplementary Materials). In this protocol, one does not need to measure \mathcal{R}_2 by observing the particle number distribution with a quantum gas microscope, and so we have more flexibility in our ability to measure \mathcal{X}_2 . Another interesting observable which is easy to measure in the ancillary qubit setting is the hopping operator $X \equiv a_j a_\ell^\dagger + \text{h.c.}$, and accordingly $X_s = \frac{1}{2} (a_{1,j} a_{1,\ell}^\dagger + a_{2,j} a_{2,\ell}^\dagger) + \text{h.c.}$ which satisfies $\mathcal{X}_2 = X_s$.

We are often interested in local observables X , which in turn correspond to the local observables X_s . Suppose that X is supported on a subregion R . Then X_s is supported on the joint region $R_1 \cup R_2$ of the two corresponding system copies. For concreteness, suppose our system is one-dimensional. We desire to measure

$$\text{tr}\{X \rho(T/2)\} = \text{tr}_R\{X \rho_R(T/2)\},$$

where $\rho_R(T/2) = \text{tr}_{\bar{R}}\{\rho(T/2)\}$ is the reduced density matrix of $\rho(T/2)$ on R . Naïvely, it seems that we only need to perform our procedure on the subsystem $R_1 \cup R_2$ of the two copies. However, this is not correct, since

$$\frac{\rho_R^2}{\text{tr}_R\{\rho_R^2\}} \neq \text{tr}_{\bar{R}}\left\{\frac{\rho^2}{\text{tr}\{\rho^2\}}\right\} = \text{tr}_{\bar{R}}\{\rho(T/2)\}.$$

Nonetheless, suppose we extend R by buffering each of its boundaries by a number of sites corresponding to the correlation length of the system at temperature $T/2$. Let us denote this extended region by B . Here, $R \subset B$, but B is smaller than the whole system. The corresponding joint region of the two system copies is $B_1 \cup B_2$. If we perform our procedure on the subsystem $B_1 \cup B_2$ of the two copies, we can access the state $\sigma_B \equiv \rho_B^2 / \text{tr}_B\{\rho_B^2\}$, which satisfies $\sigma_B \approx \text{tr}_{\bar{R}}\{\rho(T/2)\}$, and therefore

$$\text{tr}_B\{X \sigma_B\} \approx \text{tr}\{X \rho(T/2)\}.$$

So if we choose B large enough (but in most cases, smaller than the size of the entire system), we can still approximately measure our desired observable.

In an experiment, the performance of a measurement protocol is limited by the number of repetitions required to achieve sufficiently high precision. In our setting, the measurement statistics required to precisely measure the denominator $Z_n = \text{tr}\{\rho(T)^n\}$ in Eqn. (1) may be a limiting factor. In a many-body system, Z_n is directly related to the Rényi- n entropy $S_n = \frac{1}{1-n} \log(Z_n)$, which scales with volume for local systems. Z_n is therefore often exponentially small in the system size. Hence, one would generally need a large number of measurements $N_m \sim 1/Z_n^2 \sim \exp\{2s(T)|R|\}$, where $s(T)$ is the entropy density at temperature T and $|R|$ is the size of the subregion on which $\rho(T)$ is supported. In the limit of low temperature, this scaling becomes favorable since

$s(T)$ generally decreases. However, the thermal correlation length $\xi(T/n)$ can increase as T is lowered, requiring a larger subregion size $|R| \geq \xi(T/n)$. Together, the number of measurements required to achieve some fixed precision scales as $N_m \sim \exp\{2s(T)\xi(T/n)\}$.

Of course, if ρ is only approximately thermal, then expectation values of $\rho^n/\text{tr}\{\rho^n\}$ for larger values of n can have amplified deviations from thermality. However, if we are interested in the physics of the ground state $|\psi_0\rangle$, then $\rho^n/\text{tr}\{\rho^n\} \sim |\psi_0\rangle\langle\psi_0|$ for larger values of n so long as $|\psi_0\rangle$ is the dominant eigenstate of ρ . We discuss a related idea for ground state distillation in the following section.

GROUND STATE DISTILLATION

The above ideas can be generalized to schemes that not only allow us to measure a system at reduced temperatures, but further enable the distillation of the ground state from multiple copies of a thermal ensemble. This is akin to entanglement purification proposals for quantum communication over noisy channels [50]. Consider a non-destructive measurement of the swap operator, S_2 , on two systems which are each prepared in the state ρ . Since S_2 is unitary and hermitian, the two possible measurement outcomes are ± 1 , corresponding to projections into the symmetric or anti-symmetric subspace with respect to the exchange of the two copies. The state after such a measurement is thus given by $\mathcal{P}_\pm(\rho \otimes \rho)/\text{tr}\{\mathcal{P}_\pm(\rho \otimes \rho)\}$, with $\mathcal{P}_\pm = (1 \pm S_2)/2$. If the measurement outcome is -1 , we discard both systems. But for those instances that yield a measurement $+1$ we retain one of the systems, and discard only the other one. The resulting state of this first system ρ_1 is obtained by tracing out the degrees of freedom of the second system,

$$\rho_1 = \frac{\text{tr}_2\{\mathcal{P}_+(\rho \otimes \rho)\mathcal{P}_+\}}{\text{tr}\{\mathcal{P}_+(\rho \otimes \rho)\}} = \frac{\rho + \rho^2}{1 + \text{tr}\{\rho^2\}}. \quad (6)$$

For an initial thermal state $\rho(T)$, the new state ρ_1 corresponds to a mixture of $\rho(T)$ and $\rho(T/2)$. Clearly, ρ_1 has the same eigenvectors as ρ , but with different eigenvalues. In particular, ρ_1 is purer than ρ , and the eigenvalue of the largest eigenvector (i.e. the ground state for thermal ρ) is larger. This purification is of course probabilistic, as its success is conditioned on the proper measurement outcome for S_2 . Remarkably, the success probability $p_+ = (1 + \text{tr}\{\rho^2\})/2$ is always larger than $1/2$ and approaches 1 as the system is purified. Starting with multiple copies one can iterate the above process, which will ultimately converge to a system in the largest eigenstate of ρ . For thermal states, the procedure distills the many-body ground state, i.e. the zero-temperature state.

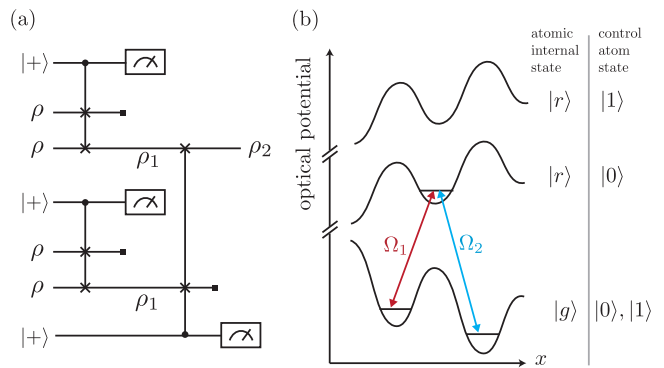


FIG. 3: (a) Quantum circuit representation of ground state distillation protocol. Following the controlled swap of two copies of a quantum state, the control ancilla qubit is measured. This protocol can be parallelized and nested, as shown in the diagram. (b) The controlled swap operation can be implemented for ultra-cold atoms on an optical lattice by the combination of photon-assisted hopping and the Rydberg blockade mechanism; excitation of the control atom in a Rydberg state conditionally prevents photon-assisted hopping.

In a cold atom setup, non-destructive measurements of the swap operator are typically more challenging to implement than the direct measurements which form the basis of the virtual cooling scheme discussed earlier. One way to realize such measurements is to use ancillary qubits [51]. For example, one can envision encoding a qubit in two internal states of an ancillary atom. Employing the Rydberg blockade mechanism, one can then use this qubit, e.g. to control the tunneling amplitude between two copies in optical lattices and so realize a controlled exchange operation (see Fig. 3 and [51]).

DISCUSSION

Reaching low temperatures is paramount for studying interesting quantum many-body phases with quantum simulators. In particular, the small energy scales in cold atom systems pose a major challenge for accessing the required temperature regimes. In this work, we proposed and demonstrated novel techniques that enable access to properties of a system at a fraction of its actual temperature. This virtual cooling is enabled by collective measurements on multiple copies of the system.

More generally, our schemes illustrate a connection between thermal physics and entanglement. In particular, the temperature of a system is intimately connected to its entanglement with its surroundings [28, 44, 45, 49, 52, 53]. Accordingly, measuring correlations of a thermal system at virtually lower temperatures involves manipulating and probing entanglement. This is why the tools for measuring a system at virtually lower temperatures resemble those that allow access to entanglement entropies [27, 40, 41].

A natural future direction is to experimentally perform quantum virtual cooling for more complicated observables. A particularly interesting application would be to experimentally study a quantum many-body system with a finite-temperature phase transition at some temperature T_c . One could prepare the system at some temperature $T > T_c$, and use virtual cooling to probe features at or below the phase transition. (For related theoretical work, see [55].) Understanding the range of applicability of quantum virtual cooling is an exciting theoretical and experimental program, which will require new insights in subsystem ETH and thermalization.

Acknowledgments. We thank Alex Avdoshkin for helpful conversations. JC is supported by the Fannie and John Hertz Foundation and the Stanford Graduate Fellowship program. SC acknowledges support from the Miller Institute for Basic Research in Science. AL, RS and MG are supported by the NSF, the Gordon and Betty Moore Foundations EPiQS Initiative, and the Air Force Office of Scientific Research MURI program. HG was supported in part by NSF grant PHY-1720397. MR was supported by an NSF Graduate Research Fellowship. PMP acknowledges funding through the ERC consolidator grant 725636 and the Daimler and Benz foundation. TG is supported as an Alfred P. Sloan Research Fellow. HP is supported by the NSF through a grant for the Institute for Theoretical Atomic, Molecular, and Optical Physics at Harvard University and the Smithsonian Astrophysical Observatory. PH was supported by AFOSR (FA9550-16-1-0082), CIFAR and the Simons Foundation.

* Electronic address: jcotler@stanford.edu

- [1] Lloyd, Seth. “Universal quantum simulators.” *Science* (1996): 1073-1078.
- [2] Gross, Christian, and Immanuel Bloch. “Quantum simulations with ultracold atoms in optical lattices.” *Science* 357.6355 (2017): 995-1001.
- [3] Georgescu, I. M., Sahel Ashhab, and Franco Nori. “Quantum simulation.” *Reviews of Modern Physics* 86 (2014): 153.
- [4] Jurcevic, Petar, et al. “Quasiparticle engineering and entanglement propagation in a quantum many-body system.” *Nature* 511 (2014): 202.
- [5] Zhang, Jiehang, et al. “Observation of a many-body dynamical phase transition with a 53-qubit quantum simulator.” *Nature* 551 (2017): 601.
- [6] Guardado-Sanchez, Elmer, et al. “Probing the Quench Dynamics of Antiferromagnetic Correlations in a 2D Quantum Ising Spin System.” *Physical Review X* 8 (2018): 021069.
- [7] Lienhard, Vincent, et al. “Observing the Space-and Time-Dependent Growth of Correlations in Dynamically Tuned Synthetic Ising Models with Antiferromagnetic Interactions.” *Physical Review X* 8 (2018): 021070.
- [8] Bernien, Hannes, et al. “Probing many-body dynamics on a 51-atom quantum simulator.” *Nature* 551 (2017): 579.
- [9] Barends, Rami, et al. “Digitized adiabatic quantum computing with a superconducting circuit.” *Nature* 534 (2016): 222.
- [10] Eichler, C., et al. “Exploring interacting quantum many-body systems by experimentally creating continuous matrix product states in superconducting circuits.” *Physical Review X* 5 (2015): 041044.
- [11] Devoret, Michel H., and Robert J. Schoelkopf. “Superconducting circuits for quantum information: an outlook.” *Science* 339.6124 (2013): 1169-1174.
- [12] Jaksch, Dieter, et al. “Cold bosonic atoms in optical lattices.” *Physical Review Letters* 81 (1998): 3108.
- [13] Greiner, Markus, et al. “Quantum phase transition from a superfluid to a Mott insulator in a gas of ultracold atoms.” *Nature* 415 (2002): 39.
- [14] Köhl, Michael, et al. “Fermionic atoms in a three dimensional optical lattice: Observing Fermi surfaces, dynamics, and interactions.” *Phys. Rev. Lett.* 94 (2005): 080403.
- [15] Aidelsburger, Monika, et al. “Realization of the Hofstadter Hamiltonian with ultracold atoms in optical lattices.” *Physical Review Letters* 111 (2013): 185301.
- [16] Miyake, Hirokazu, et al. “Realizing the Harper Hamiltonian with laser-assisted tunneling in optical lattices.” *Physical Review Letters* 111 (2013): 185302.
- [17] Stuhl, B. K. et al. “Visualizing edge states with an atomic Bose gas in the quantum Hall regime”, *Science* 349.6255 (2015): 1514
- [18] Mancini, M. et al “Observation of chiral edge states with neutral fermions in synthetic Hall ribbons”, *Science* 349.6255, (2015): 1510
- [19] Baier, Simon, et al. “Extended Bose-Hubbard models with ultracold magnetic atoms.” *Science* 352.6282 (2016): 201-205.
- [20] Simon, Jonathan, et al. “Quantum simulation of antiferromagnetic spin chains in an optical lattice.” *Nature* 472 (2011): 307.
- [21] Greif, Daniel, et al. “Short-range quantum magnetism of ultracold fermions in an optical lattice.” *Science* 340 (2013): 1307.
- [22] Hart, Russell A., et al. “Observation of antiferromagnetic correlations in the Hubbard model with ultracold atoms.” *Nature* 519, (2015): 211.
- [23] Parsons, Maxwell F., et al. “Site-resolved measurement of the spin-correlation function in the Fermi-Hubbard model”, *Science* 353:6305, (2016): 1253
- [24] Boll, Martin, et al. “Spin- and density-resolved microscopy of antiferromagnetic correlations in Fermi-Hubbard chains.” *Science* 353.6305 (2016): 1257
- [25] Cheuk, Lawrence W. et al. “Observation of spatial charge and spin correlations in the 2D Fermi-Hubbard model” *Science* 353.6305 (2016): 1260.
- [26] Mazurenko, Anton, et al. “A cold-atom Fermi-Hubbard antiferromagnet.” *Nature* 545 (2017): 462.
- [27] Islam, Rajibul, et al. “Measuring entanglement entropy in a quantum many-body system.” *Nature* 528 (2015): 77.
- [28] Kaufman, Adam M., et al. “Quantum thermalization through entanglement in an isolated many-body system.” *Science* 353.6301 (2016): 794.
- [29] Brydges, Tiff, et al. “Probing entanglement entropy via randomized measurements.” *arXiv:1806.05747* (2018).
- [30] Cheneau, Marc et al. “Light-cone-like spreading of cor-

- relations in a quantum many-body system.” *Nature* 481 (2012): 484
- [31] Meinert, Florian, et al. “Observation of many-body dynamics in long-range tunneling after a quantum quench.” *Science* 344.6189 (2014): 1259.
- [32] Schreiber, Michael, et al. “Observation of many-body localization of interacting fermions in a quasi-random optical lattice.” *Science* 349 (2015): 842.
- [33] Zeiher, Johannes, et al. “Coherent many-body spin dynamics in a long-range interacting Ising chain.” *Phys. Rev. X* 7 (2017): 041063.
- [34] Lukin, Alexander, et al. “Probing entanglement in a many-body-localized system.” *arXiv:1805.09819* (2018).
- [35] Chu, Christie et al. “Quantum State Engineering of a Hubbard System with Ultracold Fermions”, *Physical Review Letters* 120 (2018): 243201
- [36] Ho, Tin-Lun et al. “Squeezing out the entropy of fermions in optical lattices.” *PNAS* 106.17 (2009): 6916
- [37] Kantian, Adrian et al. “Dynamical Disentangling and Cooling of Atoms in Bilayer Optical Lattices.” *Physical Review Letters* 120 (2018): 060401
- [38] Ekert, Artur K., et al. “Direct estimations of linear and nonlinear functionals of a quantum state.” *Physical Review Letters* 88 (2002): 217901.
- [39] Brun, Todd A. “Measuring polynomial functions of states.” *Quantum Information & Computation* 4.5 (2004): 401.
- [40] Alves, C. Moura, and D. Jaksch. “Multipartite entanglement detection in bosons.” *Physical Review Letters* 93 (2004): 110501.
- [41] Daley, A. J., et al. “Measuring entanglement growth in quench dynamics of bosons in an optical lattice.” *Physical Review Letters* 109 (2012): 020505.
- [42] Pichler, Hannes, et al. “Thermal versus entanglement entropy: a measurement protocol for fermionic atoms with a quantum gas microscope.” *New Journal of Physics* 15.6 (2013): 063003.
- [43] J. M. Deutsch. Quantum statistical mechanics in a closed system. *Physical Review A*, 43 (1991): 2046
- [44] Mark Srednicki. Chaos and quantum thermalization. *Physical Review E*, 50 (1994): 888
- [45] Mark Srednicki. The approach to thermal equilibrium in quantized chaotic systems. *Journal of Physics A: Mathematical and General*, 32 (1999):1163.
- [46] Marcos Rigol, Vanja Dunjko, and Maxim Olshanii. Thermalization and its mechanism for generic isolated quantum systems. *Nature*, 452 (2008): 854
- [47] D’Alessio, Luca, et al. “From quantum chaos and eigenstate thermalization to statistical mechanics and thermodynamics.” *Advances in Physics* 65.3 (2016): 239.
- [48] Singh, Rajiv RP, et al. “Finite-temperature critical behavior of mutual information.” *Physical Review Letters* 106 (2011): 135701.
- [49] Garrison, James R., and Tarun Grover. “Does a single eigenstate encode the full Hamiltonian?” *Physical Review X* 8 (2018): 021026.
- [50] Duan, L.-M., et al. “Long-distance quantum communication with atomic ensembles and linear optics.” *Nature* 414 (2001): 413.
- [51] Pichler, Hannes, et al. “Measurement protocol for the entanglement spectrum of cold atoms.” *Physical Review X* 6 (2016): 041033.
- [52] Lea F. Santos, Anatoli Polkovnikov, and Marcos Rigol “Weak and strong typicality in quantum systems.” *Physical Review E* 86 (2012): 010102.
- [53] Deutsch, J. M., Li, Haibin and Sharma, Auditya “Microscopic origin of thermodynamic entropy in isolated systems” *Physical Review E* 87 (2013): 042135.
- [54] Singh, Rajiv R. P. and Hastings, Matthew B. and Kallin, Ann B. and Melko, Roger G. “Finite-Temperature Critical Behavior of Mutual Information” *Physical Review Letters* 106 (2011): 135701.
- [55] Fratus, Keith R., and Syrian V. Truong. “Does a Single Eigenstate of a Hamiltonian Encode the Critical Behaviour of its Finite-Temperature Phase Transition?” *arXiv:1810.11092* (2018).
- [56] Note that a particle number superselection rule is required for Eqn. (2).

SUPPLEMENTARY MATERIALS

I. Additional Methods for Quantum Virtual Cooling

Here we present detailed quantum virtual cooling schemes, including alternative ones that do not appear in the main text. We analyze the case of two system copies, so that quantum virtual cooling allows us to probe observables at half of the physical temperature. We start with a more general method involving an ancilla qubit, and then specialize to bosons and fermions in optical lattices.

Using an ancilla qubit

Suppose we have two identical systems, each in the same state ρ and with Hilbert spaces \mathcal{H} , and an ancilla qubit with Hilbert space \mathbb{C}^2 . The joint Hilbert space of the entire system is $\mathbb{C}^2 \otimes \mathcal{H}_1 \otimes \mathcal{H}_2$ with $\mathcal{H} \simeq \mathcal{H}_1 \simeq \mathcal{H}_2$. We define the ancilla states

$$\begin{aligned} |+\rangle &:= \frac{1}{\sqrt{2}} (|0\rangle + |1\rangle), & |-\rangle &:= \frac{1}{\sqrt{2}} (|0\rangle - |1\rangle) \\ |L\rangle &:= \frac{1}{\sqrt{2}} (|0\rangle - i|1\rangle), & |R\rangle &:= \frac{1}{\sqrt{2}} (|0\rangle + i|1\rangle). \end{aligned}$$

By jointly manipulating the ancillas and two identical systems, we will show how to measure $\text{tr}\{X \rho^2\}/\text{tr}\{\rho^2\}$ for any observable X .

The basic mathematical trick is that $\text{tr}\{S_2 \rho^{\otimes 2}\} = \text{tr}\{\rho^2\}$, and similarly $\text{tr}\{(X \otimes \mathbf{1}) S_2 \rho^{\otimes 2}\} = \text{tr}\{X \rho^2\}$. As explained in the main text, S_2 is an operator which swaps \mathcal{H}_1 and \mathcal{H}_2 by $S_2|\psi_1\rangle \otimes |\psi_2\rangle = |\psi_2\rangle \otimes |\psi_1\rangle$. In our protocol, the ancilla qubit simply provides a tool to apply the swap operator via a post-selected measurement of the state of the ancilla. We require the non-unitary ingredient of post-selection because the mapping $\rho^{\otimes 2} \rightarrow S_2 \rho^{\otimes 2}$ is non-unitary (e.g., in contrast with $\rho^{\otimes 2} \rightarrow S_2 \rho^{\otimes 2} S_2^\dagger$).

The procedure is as follows:

1. Start with the initial state $|+\rangle\langle+| \otimes \rho \otimes \rho$.
2. Apply to the joint system a controlled- $(U \otimes \mathbf{1})$ gate

$$|0\rangle\langle 0| \otimes \mathbf{1} \otimes \mathbf{1} + |1\rangle\langle 1| \otimes U \otimes \mathbf{1}, \quad (7)$$

for some unitary U on the first system copy, followed by a controlled- S_2 gate

$$|0\rangle\langle 0| \otimes \mathbf{1} \otimes \mathbf{1} + |1\rangle\langle 1| \otimes S_2, \quad (8)$$

where the control qubit is the ancilla.

3. Measure the ancilla qubit in the $\{|+\rangle, |-\rangle\}$ and $\{|L\rangle, |R\rangle\}$ bases, respectively, to obtain the measurement probabilities:

$$\text{Prob}(\pm) = \frac{1}{2} (1 \pm \text{Re}[\text{tr}\{U \rho^2\}]) \quad (9)$$

$$\text{Prob}(L/R) = \frac{1}{2} (1 \pm \text{Im}[\text{tr}\{U \rho^2\}]) . \quad (10)$$

These probabilities can be used to reconstruct $\text{tr}\{U \rho^2\}$ for any chosen unitary U .

4. Let $\{U_i\}$ be an orthogonal basis (i.e., $\text{tr}\{U_i^\dagger U_j\} = \dim(\mathcal{H}_2) \cdot \delta_{ij}$) for $\mathcal{B}(\mathcal{H}_2)$. For instance, if the two system copies are comprised of qubits or qudits, one could use strings of Pauli operators or generalized Pauli operators. Then using the first three steps above, for *any* operator $X \in \mathcal{B}(\mathcal{H}_2)$, one can compute $\text{tr}\{X \rho^2\}/\text{tr}\{\rho^2\}$ using the relation

$$\frac{\text{tr}\{X \rho^2\}}{\text{tr}\{\rho^2\}} = \frac{1}{\dim \mathcal{H}_2} \sum_{i=1}^{\dim \mathcal{B}(\mathcal{H}_2)} \text{tr}\{U_i^\dagger X\} \frac{\text{tr}\{U_i \rho^2\}}{\text{tr}\{\rho^2\}} . \quad (11)$$

The last step may seem daunting, since the sum in Eqn. (11) contains $\dim \mathcal{B}(\mathcal{H}_2) = (\dim \mathcal{H}_2)^2$ terms. However, a good choice of $\{U_i\}$ renders only a few terms in the sum non-zero. For instance, suppose that the two identical systems are each spin chains of qubits, and that X is a product two Pauli operators, each on a separate site. If $\{U_i\}$ is chosen to be products of Pauli operators, then only one term in the sum would be non-zero (namely the term for which $U_i^\dagger = X$).

Boson interferometry

If our two identical systems are bosonic, then we can perform quantum virtual cooling along the lines of the main text. In particular, we do not need an ancilla qubit to facilitate the application of the swap operator. Consider the bosonic Hilbert space $\text{Sym}(\mathcal{H}_1 \otimes \mathcal{H}_2)$, comprising of two systems with N sites each. A basis for $\text{Sym}(\mathcal{H}_1 \otimes \mathcal{H}_2)$ is

$$|\{p_i\}, \{q_j\}\rangle = \prod_{i,j=1}^N (a_{2,i}^\dagger - a_{1,i}^\dagger)^{p_i} (a_{2,j}^\dagger + a_{1,j}^\dagger)^{q_j} |\text{vac}\rangle \quad (12)$$

for $\{p_i\}, \{q_j\} \in \mathbb{Z}_{\geq 0}^{\times N}$. From Eqn. (2), \mathcal{F}_2 is a unitary which maps

$$\mathcal{F}_2 \frac{1}{\sqrt{2}} (a_{2,i}^\dagger + a_{1,i}^\dagger) \mathcal{F}_2^\dagger = a_{2,i}^\dagger \quad (13)$$

$$\mathcal{F}_2 \frac{1}{\sqrt{2}} (a_{2,i}^\dagger - a_{1,i}^\dagger) \mathcal{F}_2^\dagger = a_{1,i}^\dagger. \quad (14)$$

Furthermore, $\mathcal{R}_2 = (-1)^{\sum_j n_{1,j}}$ is the total parity operator for the first of the two identical systems. It is easy to check that

$$S_2 |\{p_i\}, \{q_j\}\rangle = \mathcal{F}_2^\dagger \mathcal{R}_2 \mathcal{F}_2 |\{p_i\}, \{q_j\}\rangle, \quad (15)$$

and so

$$\text{tr}\{\mathcal{R}_2 \mathcal{F}_2 \rho^{\otimes 2} \mathcal{F}_2^\dagger\} = \text{tr}\{S_2 \rho^{\otimes 2}\} = \text{tr}\{\rho^2\}. \quad (16)$$

Then if we have an operator X that we wish to measure, the idea is to instead measure $\mathcal{X}_2 = \mathcal{F}_2 \frac{1}{2} (X \otimes \mathbf{1} + \mathbf{1} \otimes X) \mathcal{F}_2^\dagger$ so that, in essence,

$$\text{tr}\{\mathcal{R}_2 \mathcal{X}_2 \mathcal{F}_2 \rho^{\otimes 2} \mathcal{F}_2^\dagger\} = \frac{1}{2} \text{tr}\{\mathcal{R}_2 \mathcal{F}_2 (X \otimes \mathbf{1} + \mathbf{1} \otimes X) \rho^{\otimes 2} \mathcal{F}_2^\dagger\} = \frac{1}{2} \text{tr}\{S_2 (X \otimes \mathbf{1} + \mathbf{1} \otimes X) \rho^{\otimes 2}\} = \text{tr}\{X \rho^2\}. \quad (17)$$

Of course, there is a detailed measurement procedure which realizes the above equations.

To measure $\text{tr}\{X \rho^2\}/\text{tr}\{\rho^2\}$, we use the following procedure:

1. Start with the initial state $\rho^{\otimes 2}$.
2. Apply \mathcal{F}_2 to obtain

$$\sum_i \mathcal{F}_2 \rho^{\otimes 2} \mathcal{F}_2^\dagger. \quad (18)$$

3. Measure the operator \mathcal{X}_2 , given by

$$\mathcal{X}_2 = \mathcal{F}_2 \left(\frac{1}{2} X(\{a_{1,i}, a_{1,i}^\dagger\}) + \frac{1}{2} X(\{a_{2,i}, a_{2,i}^\dagger\}) \right) \mathcal{F}_2^\dagger. \quad (19)$$

Here, $X(\{a_{1,i}, a_{1,i}^\dagger\})$ denotes that the operator is written in terms of sums of products of creation and annihilation operators in the set $\{a_{1,i}, a_{1,i}^\dagger\}_{i \in \text{sites}}$, and similarly for $X(\{a_{2,i}, a_{2,i}^\dagger\})$. The operator \mathcal{X}_2 has the property $[\mathcal{X}_2, \mathcal{R}_2] = 0$, which will be utilized shortly. Suppose $\mathcal{X}_2 = \sum_i \lambda_i P_i$ where the $\{P_i\}$ are orthogonal projectors. Then after measurement one is left with

$$\sum_i P_i \mathcal{F}_2 \rho^{\otimes 2} \mathcal{F}_2^\dagger P_i. \quad (20)$$

4. Measure $\mathcal{R}_2 = \Pi_+ - \Pi_-$ (where Π_{\pm} is the projector onto the \pm eigenspace) to obtain

$$\sum_i \Pi_+ P_i \mathcal{F}_2 \rho^{\otimes 2} \mathcal{F}_2^\dagger P_i \Pi_+ + \sum_i \Pi_- \mathcal{F}_2 P_i \rho^{\otimes 2} P_i \mathcal{F}_2^\dagger \Pi_- . \quad (21)$$

5. The probability that one measures \mathcal{R}_2 as $+1$, after having measured $\rho^{\otimes 2}$ to be in the subspace corresponding to P_i , is denoted by $\text{Prob}(+|i)$. Similarly, the probability that one measures \mathcal{R}_2 as -1 , after having measured $\rho^{\otimes 2}$ to be in the subspace corresponding to P_i , is denoted by $\text{Prob}(-|i)$. After obtaining $\text{Prob}(+|i)$ and $\text{Prob}(-|i)$, one can compute

$$\begin{aligned} \sum_i \lambda_i \left(\text{Prob}(+|i) - \text{Prob}(-|i) \right) &= \sum_i \lambda_i \text{tr} \left\{ \Pi_+ P_i \mathcal{F}_2 \rho^{\otimes 2} \mathcal{F}_2^\dagger P_i \Pi_+ - \Pi_- \mathcal{F}_2 P_i \rho^{\otimes 2} P_i \mathcal{F}_2^\dagger \Pi_- \right\} \\ &= \sum_i \lambda_i \text{tr} \left\{ \mathcal{R}_2 P_i \mathcal{F}_2 \rho^{\otimes 2} \mathcal{F}_2^\dagger P_i \right\} \\ &= \text{tr} \{ \mathcal{R}_2 \mathcal{X}_2 \mathcal{F}_2 \rho^{\otimes 2} \mathcal{F}_2^\dagger \} \\ &= \text{tr} \{ X \rho^2 \} , \end{aligned} \quad (22)$$

where we have used $[\mathcal{X}_2, \mathcal{R}_2] = 0$ to go from the second line to the third line, and Eqn. (17) to go from the third line to the last line. A similar procedure can be used to determine $\text{tr}\{\rho^2\}$, and then one can compute the quotient $\text{tr}\{X \rho^2\}/\text{tr}\{\rho^2\}$.

In an actual experiment, one does not directly measure the parity operator \mathcal{R}_2 , but instead measures the number operator on every site. Since the common refinement of the eigenspaces of all of the number operators is a refinement of the eigenspaces of \mathcal{R}_2 , one can measure \mathcal{R}_2 via the number operators and obtain the same result as above.

Fermion interferometry

It is straightforward to adapt the boson interferometry techniques to fermions, although a few modifications to the protocol are required. Our protocol is inspired by the work of [42]. Suppose we have two systems of fermions, and require that states of different fermion number lie in different superselection sectors. Technically, the superselection rule means that for all observables X , we have $\langle \psi_1 | X | \psi_2 \rangle = 0$ if $|\psi_1\rangle$ and $|\psi_2\rangle$ are states of definite, but distinct fermion number.

For fermions, it is *not* true that $\text{tr} \left\{ \mathcal{R}_2 \mathcal{F}_2 \rho^{\otimes 2} \mathcal{F}_2^\dagger \right\} = \text{tr}\{\rho^2\}$. Instead, we have

$$\text{tr} \left\{ \mathcal{V} \mathcal{F}_2 \rho^{\otimes 2} \mathcal{F}_2^\dagger \right\} = \text{tr}\{\rho^2\} \quad (23)$$

where \mathcal{V} has eigenvalues ± 1 which depend on the total number of fermions N_{tot} , the floor of half of the total number of fermions $\lfloor N_{\text{tot}}/2 \rfloor$, and the number of fermions N_2 in the second copy of the subsystem. (There are, in fact, many choices of \mathcal{V} which satisfy Eqn. (23), and so we choose a convenient one for our purposes.) The measurement outcomes for \mathcal{V} are given in the table below:

N_{tot}	$\lfloor N_{\text{tot}}/2 \rfloor$	N_2	Result
Even	Even	Even	+1
Even	Even	Odd	-1
Even	Odd	Even	-1
Even	Odd	Odd	+1
Odd	Even	Even	+1
Odd	Even	Odd	-1
Odd	Odd	Even	-1
Odd	Odd	Odd	+1

TABLE I: Characterization of measurement outcomes for \mathcal{V} .

The procedure for measuring $\text{tr}\{\mathcal{X}_2 \rho^2\}/\text{tr}\{\rho^2\}$ is the same as in the bosonic case above, except that now we need

$$\mathcal{X}_2 = \mathcal{F}_2 \left(\frac{1}{2} X(\{f_{i,1}, f_{i,1}^\dagger\}) + \frac{1}{2} X(\{f_{i,2}, f_{i,2}^\dagger\}) \right) \mathcal{F}_2^\dagger,$$

(where here the f, f^\dagger operators are fermionic) to additionally satisfy

$$[\mathcal{X}_2, \mathcal{V}] = 0. \quad (24)$$

So first let us find which operators, in general, commute with \mathcal{V} . Suppose we have an operator of the form

$$\underbrace{f_{i_1,1}^\dagger \cdots f_{i_{m_1},1}^\dagger}_{m_1 \text{ of these}} \underbrace{f_{j_1,1} \cdots f_{j_{m_2},1}}_{m_2 \text{ of these}} \underbrace{f_{k_1,2}^\dagger \cdots f_{k_{n_1},2}^\dagger}_{n_1 \text{ of these}} \underbrace{f_{\ell_1,2} \cdots f_{\ell_{n_2},2}}_{n_2 \text{ of these}} \quad (25)$$

where $\{i_1, \dots, i_{m_1}\}, \{j_1, \dots, j_{m_2}\}, \{k_1, \dots, k_{n_1}\}, \{\ell_1, \dots, \ell_{n_2}\}$ are all sets with *non-repeating* elements. All of these operators transform multiplicatively by either $+1$ or -1 after conjugation by \mathcal{V} . Letting $m = |m_1 - m_2|$ and $n = |n_1 - n_2|$, the possibilities are tabulated below:

$m + n \pmod{2}$	$m + n \pmod{4}$	$n \pmod{2}$	Result
0	2	0	-1
0	2	1	$+1$
0	0	0	$+1$
0	0	1	-1
1	1	0	-1
1	1	1	$+1$
1	3	0	$+1$
1	3	1	-1

TABLE II: Transformation of products of fermion operators under conjugation by \mathcal{V} .

For example, letting $\mathcal{X}_2 = \frac{1}{2}(n_{i,1} + n_{i,2})$, we have $[\mathcal{X}_2, \mathcal{V}] = 0$. If instead $\mathcal{X}_2 = \mathcal{F}_2(\frac{1}{2}(n_{i,1}n_{j,1} + n_{i,2}n_{j,2}))\mathcal{F}_2^\dagger$, we likewise have $[\mathcal{X}_2, \mathcal{V}] = 0$.

II. Extracting two point correlations in the low temperature limit

In this section, we numerically study the effect of the second term in Eqn. (5) in the main text. More specifically, we have argued that one can extract a density-density correlation from a more experimentally accessible quantity:

$$C(j, \ell) \equiv \frac{1}{2} \text{tr} \{n_j n_\ell \rho(T/2)\} + \frac{1}{2} \frac{\text{tr} \{n_j \rho(T) n_\ell \rho(T)\}}{\text{tr} \{\rho(T)^2\}}. \quad (26)$$

While the first term is the desired density-density correlation, the second term arises as a consequence of the Fourier transform of local operators n_j and n_ℓ . As described in the main text, however, we expect that at sufficiently low temperatures the second term does not exhibit any systematic dependence on the distance between two points $d = |j - \ell|$, allowing us to extract physically meaningful quantities such as correlations lengths from fitting $C(j, \ell)$ as a function of d .

In order to confirm this expectation, we consider a 1D Bose-Hubbard Hamiltonian with nearest-neighbor hopping rate J and on-site repulsive interaction $U = 3J$. We numerically compute thermal density matrices for $N = 4$ particles on $L = 16$ lattice sites with periodic boundary condition at various temperature $T/J \in \{\frac{1}{10}, \frac{1}{5}, \frac{1}{4}, \frac{1}{2}, 1\}$. For each temperature T , we compute each term in $C(j, \ell)$ as well as their sum as a function of the distance $d \in \{1, \dots, 8\}$. Fig. 4 below summarizes our numerical results, from which it can be checked that the density-density correlation (the first term in $C(j, \ell)$) displays strong anti-bunching (Fig. 4a) at low temperature. By contrast, the second term exhibits diminishing distance-dependence as the temperature decreases (Fig. 4b). We find that the distance dependence of the total value $C(j, \ell)$ is indeed dominated by the density-density correlation (Fig. 4c) at sufficiently low temperatures.

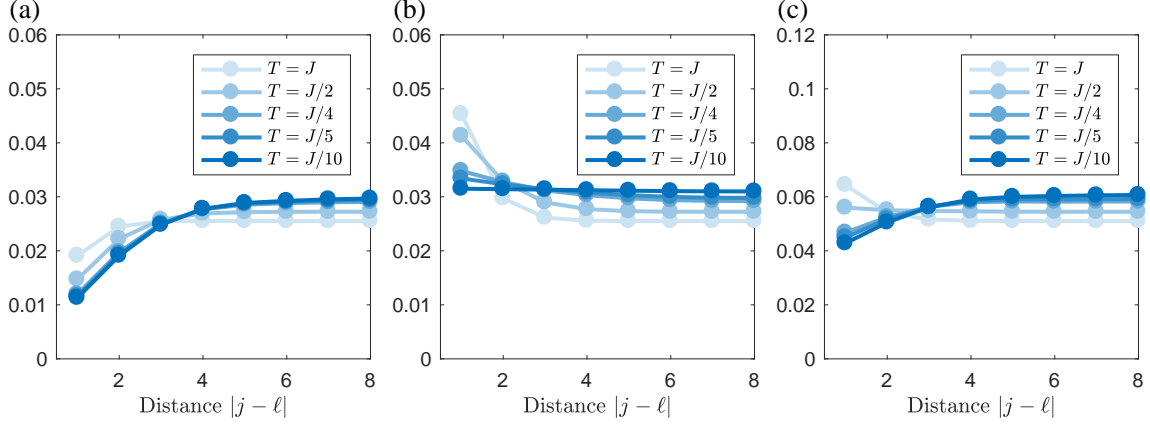


FIG. 4: Extracting the density-density correlation from Eqn. (5) in the main text. (a) Density-density correlations in a 1D Bose-Hubbard model at various temperatures. This quantity corresponds to the first term in $C(j, \ell)$. (b) Additional contribution to $C(j, \ell)$ arising from the second term. Crucially, this contribution exhibits decreasing distance-dependence in the low temperature limit. (c) The position dependence of the total value $C(j, \ell)$ is dominated by the first term in low temperature limit.

III. Experimental methods

Our experiments start from a high fidelity Mott insulator with a single particle per lattice site. Using high-precision, site-resolved optical potentials, created by a digital micro-mirror device (DMD), we isolate two neighboring six-site long chains of atoms with exactly one atom on each site. In order to ensure the high fidelity of the initial state we hold it in the $45E_r$ deep optical lattice in both directions. To obtain a locally thermal state we suddenly drop the lattice depth along the chains, allowing atoms to tunnel, while keeping the lattice high between the chains. We use a pair of DMD beams to offset the sites right outside the region of interest, thereby defining the overall length of the system. After variable evolution time, we freeze the dynamics along the chains by suddenly ramping up the lattice back to $45E_r$. In order to make sure that the state has thermalized, we pick evolution times for which the entanglement entropy of the region of interest has reached its saturation value. Table III shows the times used in Fig. 2 in the main text for each case studied.

Case	Times (\hbar/J)
A	1.0, 1.4, 2.2, 4.3, 5.1, 6.4, 8.4
B	12.2, 24.0, 59.4
C	22.4, 41.3

TABLE III: Evolution times used for each case in Fig. 2 of main text.

In order to implement the beamsplitter operation, we drop the lattice depth between the chains and let the atoms evolve for a certain time duration. During this process the lattice depth along the chains stays high, preventing wavefunction evolution in that direction. At the end of this sequence, we read out the state of the system in the particle number basis with single-site and full atom-number resolution. For more details see [28].